JMEPEG (2011) 20:830–834
DOI: 10.1007/s11665-010-9758-2

1059-9495/$19.00

Comparison of Optical and SEM-BEI Inclusion Analyses of VIM-VAR Nickel-Titanium Alloy

Frank Sczerzenie, Graeme W. Paul, Clarence Belden, and Audrey Fasching

(Submitted May 11, 2010; in revised form July 28, 2010)

The ASTM Standard for NiTi alloys does not specify the method to be used for the analysis of inclusions. Quantitative analysis is generally done by optical metallography with a computer program to measure size and area fraction. This study gives a comparison of quantitative analyses of inclusions by scanning electron microscopy using backscattered electron imaging (SEM-BEI) and quantitative analyses by optical metallography. Seven samples of 6.3-mm hot-rolled NiTi were evaluated. The coil samples were selected to exhibit a wide range of inclusion content. Each sample had a different Ni to Ti ratio corresponding to a different transformation temperature range (TTR) from A_s = −25 °C (Ni = 50.79 a/o) to A_s = +95 °C (Ni = 49.63 a/o). Quantitative analyses by optical and by SEM-BEI are in reasonable good agreement for maximum particle size and maximum area fraction. Both methods of analysis show that carbide and intermetallic oxide inclusion populations in VIM-VAR hot-rolled coil vary significantly in the amount and size of inclusions with the alloy transformation temperature. Therefore, an analysis of a larger number of samples at each TTR is needed to develop statistically precise data. All carbide inclusions were less than 12.5 µm and less than 1.0% area fraction in all the samples. Maximum size and area fraction of carbides decreased as TTR increased. Intermetallic oxide size and area fraction increased with increasing TTR Intermetallic oxides are fractured and separated from the matrix during hot working. However, stringering is very limited. The fracturing appears to happen in high TTR alloys but not in low TTR alloys. This dependence on TTR suggests that chemistry in or around the oxides affects their fracture behavior.

Keywords biomaterials, electron microscopy, metallography, NiTi alloy, nitinol, quantitative metallography

1. Introduction

The ASTM Standard for NiTi alloys specifies the limits for the size and area fraction of non-metallic inclusions, TiC and $Ti_4Ni_2O_x$, in the alloys. However, the Standard does not specify the method to be used for the analysis of inclusions (Ref 1). Quantitative inclusion analysis is generally done by optical metallography with a computer program to measure size and area fraction (Ref 2). A recent study by Toro et al. characterized inclusions in NiTi tubing by both scanning electron microscopy (SEM) and optical metallography (Ref 3). They reported that both carbides and oxides are isolated particles in hot-rolled vacuum induction-melted and vacuum arc-remelted (VIM-VAR) bar. They observed that fragmentation of oxides was the primary mechanism of stringer formation during cold drawing of tubing. The area of the stringer was increased by the formation of voids between oxide fragments and between oxides and adjacent carbides. Voids were also formed at the lead and tail ends of isolated carbides that became partially separated from the matrix.

The aim of this study was to compare quantitative analyses of inclusions by scanning electron microscopy using backscattered electron imaging (SEM-BEI) to quantitative analyses by optical metallography. Sczerzenie et al., have demonstrated that the type, carbide or oxide, size, and area fraction of inclusions in VIM-VAR alloy depends, in part, on the Ni to Ti ratio of the alloy (Ref 4). In order to compare the quantitative analytical capabilities of optical metallography and SEM-BEI on a wide range of inclusion size and area fractions, coils with different Ni to Ti ratios as measured by the A_s in the fully annealed condition were analyzed. To simplify the quantitative analysis, the study was limited to hot-rolled coil where fragmentation and stringering of inclusions and void formation are limited.

2. Experimental

Seven samples of 6.3 mm hot-rolled coil were evaluated. Each sample had a different transformation temperature range (TTR) corresponding to a different Ni to Ti ratio. A_s ranged from −25 °C (Ni = 50.79 a/o), to A_s = +95 °C (Ni = 49.63 a/o). The samples were taken from full size production coils. The production sequence included hot forging of 355 mm × 1700 kg VIM-VAR ingots to 102-mm diameter billets, surface conditioning and hot rolling to 6.6 mm diameter × 170 kg coils.

This article is an invited paper selected from presentations at Shape Memory and Superelastic Technologies 2010, held May 16-20, 2010, in Pacific Grove, California, and has been expanded from the original presentation.

Frank Sczerzenie, Graeme W. Paul, and **Clarence Belden**, SAES Smart Materials, New Hartford, NY 13413; and **Audrey Fasching**, SAES Memry, Menlo Park, CA 94025. Contact e-mails: Frank_Sczerzenie@saes-group.com, Graeme_Paul@saes-group.com, and Audrey_Fasching@Memry.com.

The coil samples were longitudinal centerline full diameter by 12.7 mm long as shown in Fig. 1. The samples were polished in stages through 120 grit stone, 240 grit paper, 15 μm diamond, 9 μm diamond, and finally 3 μm diamond. The samples were examined at 500× magnification on a Zeiss Observer D1M inverted stage metallography in the as-polished condition. Chemical etching or electropolishing were not used to preserve the flatness of the surface and to avoid rounding of the inclusions and expanding the porosity. In this condition, carbides and intermetallic oxides and voids can be differentiated from the matrix by color in the light microscope. The carbides are pink, the intermetallic oxides are pale blue, and the voids are black. This was confirmed in prior unpublished study by marking individual particles on the optical microscope and then transferring the samples to the SEM for EDAX confirmation of the particle chemistry.

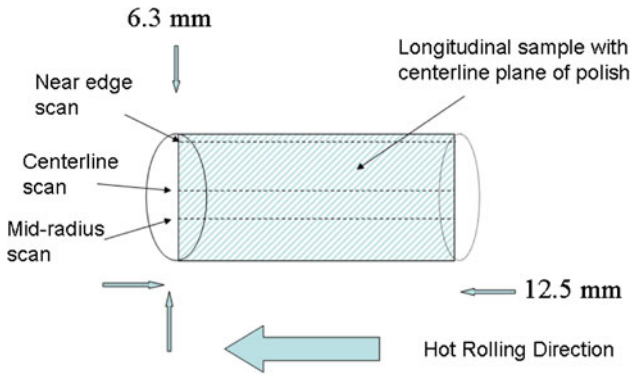

Fig. 1 Schematic of sample from coil and metallographic scanning technique

The inclusion content was quantified by scanning the length of the sample in three regions—the centerline, the mid-radius line, and the near-edge line of the cross section, as shown in Fig. 1. Three fields of view were photographed at 500× in each scan. These were chosen by the metallographer to show the largest inclusion and/or the largest area density of inclusions observed. Image-Pro Plus Version 6.3 software was used to create a digital image of each micrograph. The metallographer switched between the optical image and the computer image and adjusted the computer system to capture the image of all the particles larger than 0.1 μm in the field of view. The nine computer images for each sample were saved to the computer with the optical pictures. The quantitative metallographic program measured and recorded the largest dimension of each particle imaged to the computer. The program calculated the average dimension for each inclusion. The average dimension

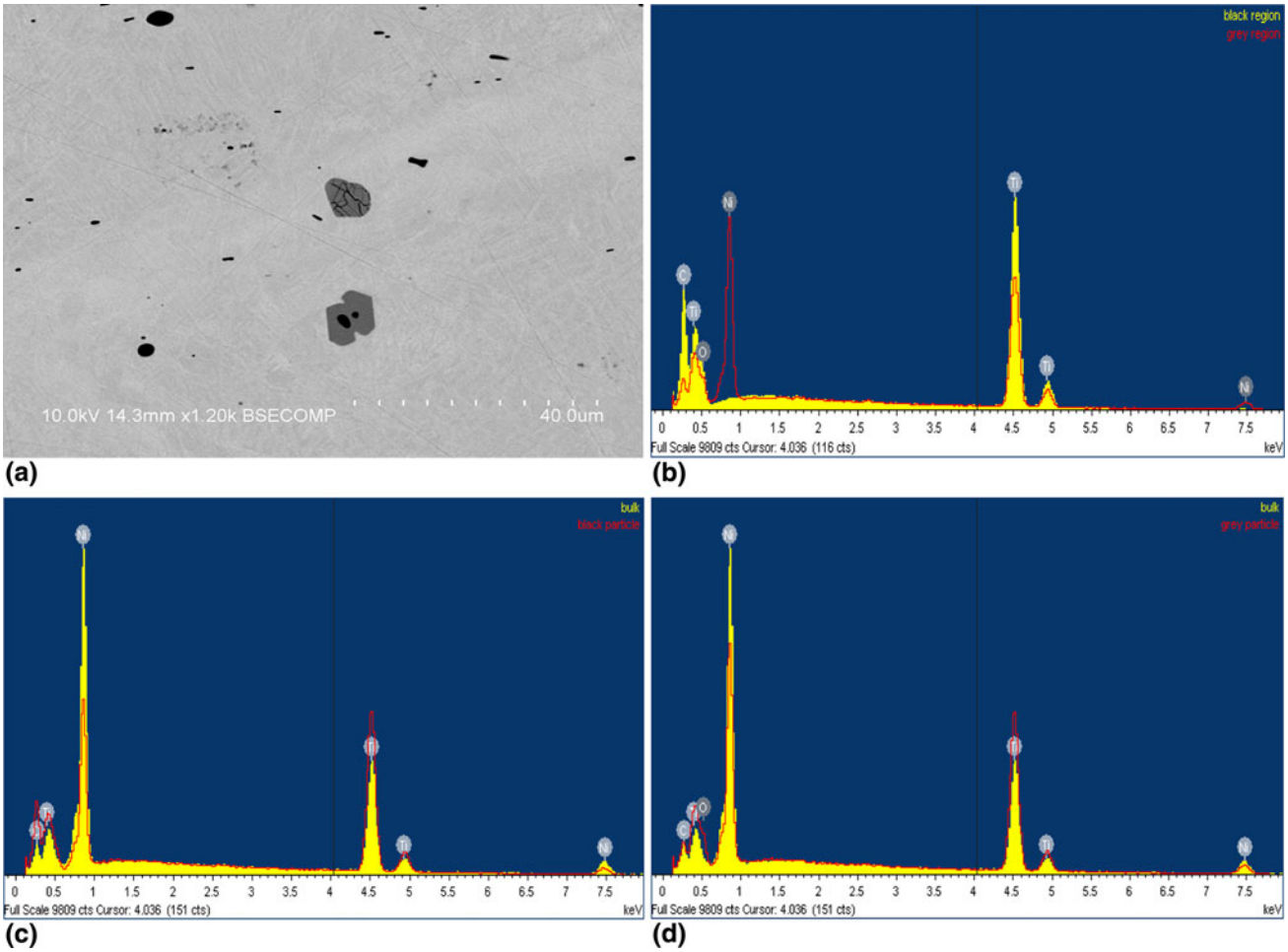

Fig. 2 C5-9261-1 (A_s = 55 °C) coil (a) carbide encapsulation and oxide fracture, (b) EDS spectra for matrix and oxide, (c) EDS spectra for carbide and matrix, and (d) EDS spectra for oxide case and encased carbide in a higher transformation temperature alloy sample

Table 1 Inclusion analysis of various NiTi transformation temperature range alloy samples by optical and SEM-BEI image analyses

		Optical metallography						SEM-BEI				
		Maximum carbide		Minimum % fields carbides <12.5 m	Maximum intermetallic		% Fields without oxide	Maximum carbide		Minimum % fields carbides <12.5 m	Maximum intermetallic		% Fields without oxide
Coil sample	A_s, °C	µm	%		µm	%		µm	%		µm	%	
C5-9927-4T	−25	11.93	0.79	100.0	0.00	0.00	100.0	9.26	0.71	100.0	4.79	0.06	88.9
C5-9926-4T	−12	7.89	0.63	100.0	9.96	0.21	0.0	8.91	0.49	100.0	11.77	0.15	11.1
C7-8591-4T	0	10.62	0.70	100.0	0.00	0.00	100.0	9.09	0.83	100.0	0.00	0.00	100.0
C7-8616-6TB	30	6.76	0.50	100.0	24.10	0.84	22.2	7.76	0.25	100.0	22.27	0.59	0.0
C5-9261-1	55	6.45	0.22	100.0	15.75	0.68	0.0	5.15	0.16	100.0	24.27	0.72	0.0
C5-9229-3T	70	10.59	0.26	100.0	16.11	0.48	0.0	6.99	0.57	100.0	18.16	0.40	0.0
C5-9287-3T	95	4.62	0.17	100.0	31.01	2.94	0.0	8.60	0.10	100.0	30.39	2.93	0.0

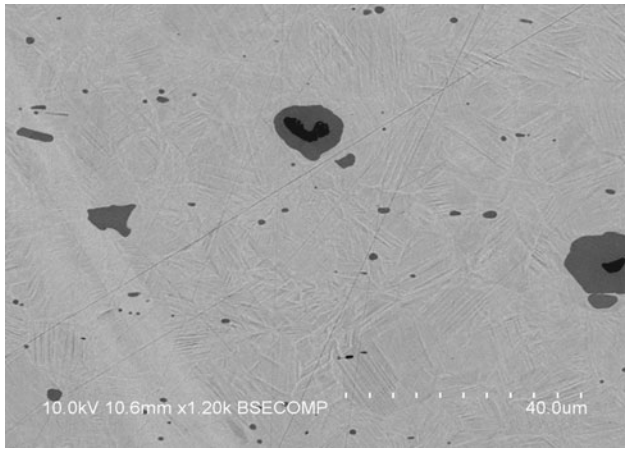

Fig. 3 C5-9287-3T (A_s = 95 °C) carbide encased in oxide in a higher transformation temperature alloy sample

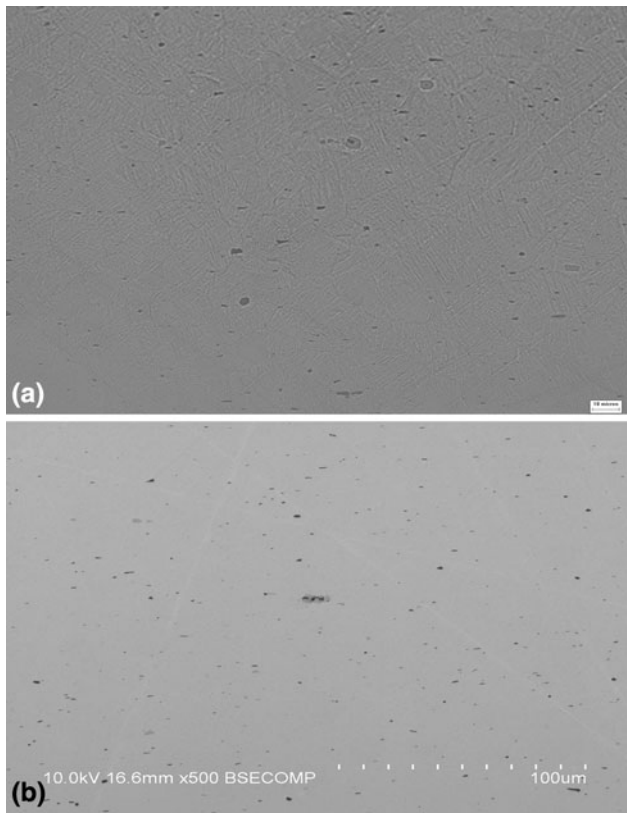

Fig. 4 C5-9926-4T (A_s = −12 °C) coil (a) optical image and (b) SEM-BEI image of a lower transformation temperature alloy sample showing typical structure

of each inclusion was used as a diameter to calculate the area of an equivalent spherical particle. The areas of all of the particles were added and divided by the total area of the image to calculate the area fraction of the inclusions.

The SEM imaging was conducted on a Hitachi S-3400N microscope using backscattered electron imaging (BEI); EDS microanalysis used a silicon drift detector (SDD) and Oxford INCA software. The inclusion content was quantified by scanning the length of the sample in three regions—the

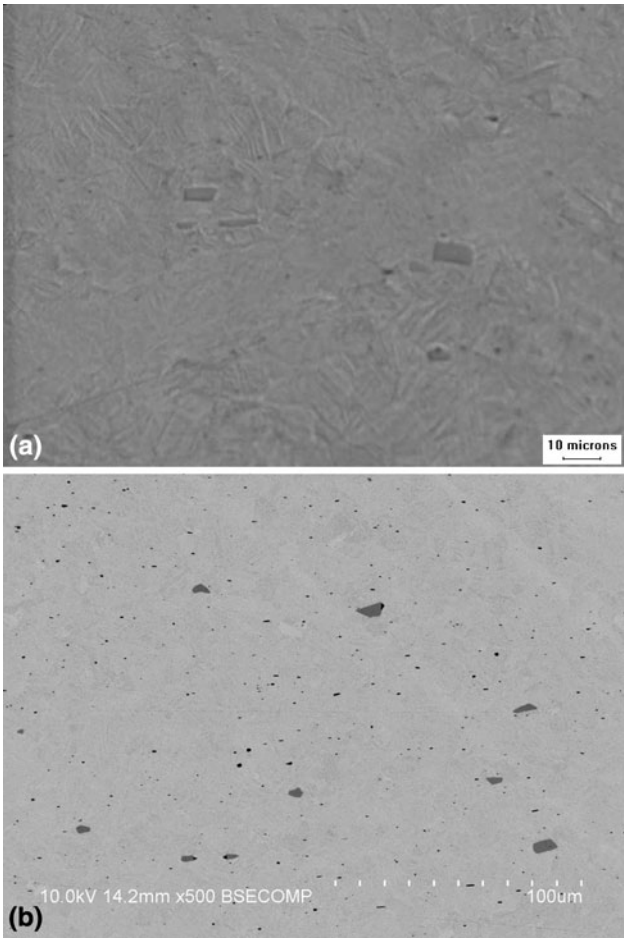

Fig. 5 C5-9261-1 (A_s = 55 °C) coil (a) optical image and (b) SEM-BEI image of a higher transformation temperature alloy sample showing typical structure

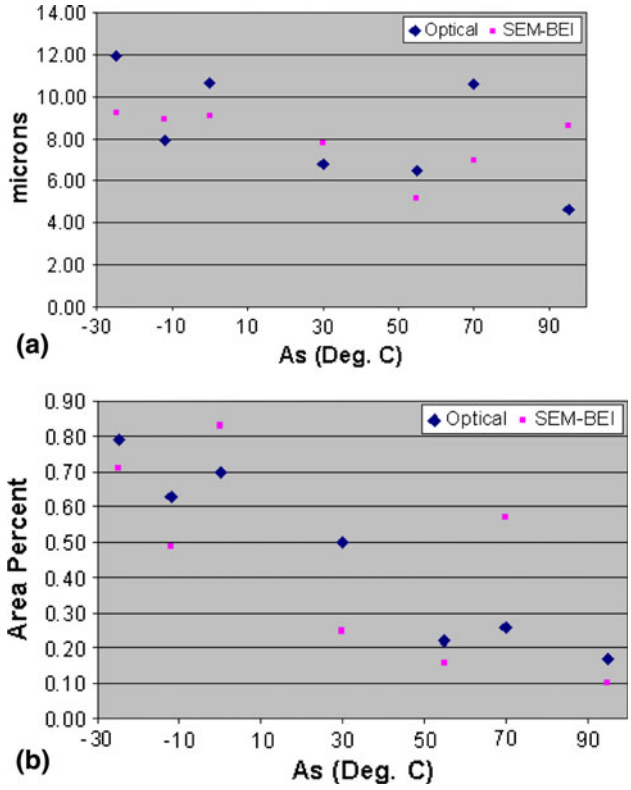

Fig. 6 (a) Maximum carbide size vs. transformation temperature range by optical and SEM-BEI image analysis. (b) Maximum carbide area fraction vs. transformation temperature range by optical and SEM-BEI image analysis

centerline, the mid-radius line, and the near-edge line of the cross section. Three fields of view were photographed at 500× in each region. The regions were chosen by the metallographer to show the largest inclusion and/or the largest area density of inclusions observed. SEM-BEI images at 500× were evaluated using the same quantitative metallographic analysis protocol as for the optical images.

EDS (electron dispersive spectroscopy) was used to analyze the chemistry of the constituents of the microstructure. Figure 2(a)-(d) shows a typical SEM-BEI image and EDS of the A_s = 95 °C coil at 1200× magnification. Figure 2(a) shows the microstructure with carbides and oxides resolved. One large oxide is fractured. Figure 2(b) shows the spectra for the NiTi bulk matrix and the gray oxide particle. Nickel was reduced, and titanium and oxygen were increased relative to the bulk matrix. Figure 2(c) shows the spectra for the black carbide particle. Carbon and titanium were increased relative to the matrix. Figure 2(d) shows the spectra for the carbide encased in oxide. The carbide had no nickel. The gray oxide had both carbon and oxygen with titanium and nickel. Larger oxides were observed to be fractured but not yet stringered in several samples. This occurred more frequently in the higher TTR samples an example of which is shown in Fig. 2. Figure 3 is a 1200× SEM photo showing two examples of carbides encased in oxide in an A_s = 95 °C alloy. The encased particles were counted as oxides, and no attempt was made to analyze the size and area of the encased carbides separately.

3. Results

Table 1 shows the inclusion analysis for the seven coil samples. Figure 4 shows typical structures for a lower TTR alloy (A_s = −12 °C) at 500×: Fig. 4(a), an optical image, shows several carbides encased in oxide; and Fig. 4(b), a SEM-BEI image of a different area of the same sample, has better contrast and shows fracture of an oxide at the center of the field of view. Figure 5 shows typical structures for higher TTR alloy (A_s = 55 °C). Higher number of and larger-sized oxides were observed in the higher TTR alloy samples compared with the lower TTR alloy samples. Figures 6 and 7 show the maximum size and maximum area fraction versus TTR, for carbides and oxides, respectively measured by both optical and SEM-BEI image analysis.

4. Discussion

The differences between the data from optical and SEM-BEI were calculated by subtracting the SEM data from the optical metallographic data for each parameter in Table 1. The differences and the average of the differences for the seven

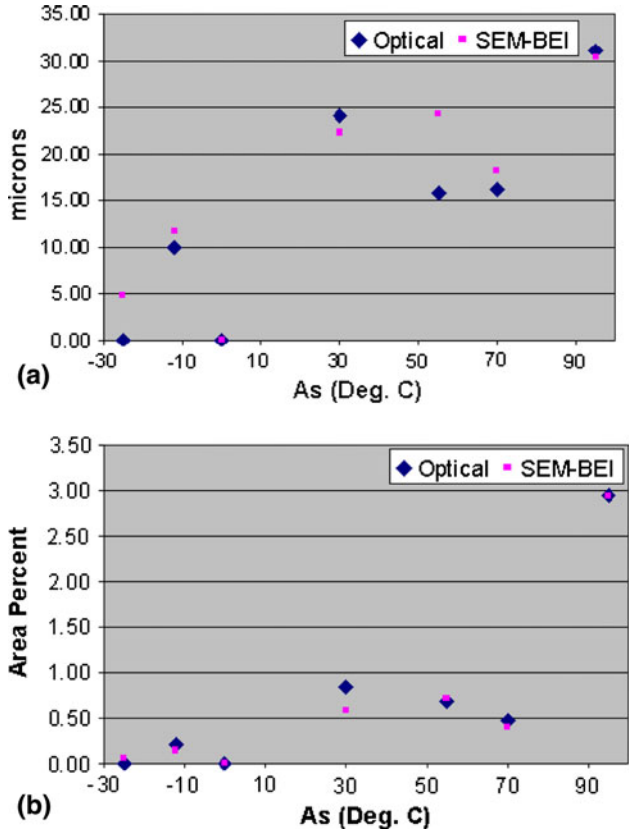

Fig. 7 (a) Maximum oxide size vs. transformation temperature range by optical and SEM-BEI image analysis. (b) Maximum area fraction of oxides vs. transformation temperature range by optical and SEM-BEI image analyses

samples are shown in Table 2. The differences in the area fractions for both carbides and oxides are very small. The average difference in carbide size is less than 1 μm. The average difference in oxide size is 2 μm and suggests that optical metallography may underestimate oxide size compared to SEM-BEI. The data show that optical and SEM-BEI analyses are in close agreement on the size and area fraction of both carbides and oxides. However, the number of samples was too small to make a firm conclusion. SEM-BEI was better for detecting very small oxides and fracture of larger oxides.

Fracture of oxides was observed in two of the higher TTR samples with A_s above 30 °C. At A_s = 30 °C and below, large oxides were not fractured, but they did separate from the matrix forming voids.

The coil samples were selected to exhibit a wide range of inclusion content. The overall trend was for maximum carbide size and area fraction to decrease, and maximum oxide size and area fraction to increase with increasing TTR. One of the lower TTR samples had no oxide inclusion as found by either optical or SEM-BEI analysis. However, the absence of intermetallic oxides was not consistent for all low TTR samples.

All carbide inclusions were less than 12.5 μm and less than 1.0% area fraction in all samples at all TTRs. This includes samples in which there are no intermetallic oxides. The maximum size and area fraction of carbides decreased as the TTR increased.

Table 2 Differences in carbide and oxide size and area faction between optical and SEM-BEI image analyses in various NiTi transformation temperature range alloy samples

		Carbide		Oxides	
Coil sample	A_s, °C	μm	Area %	μm	Area %
C5-9927-4T	−25	2.67	0.08	−4.79	−0.06
C5-9926-4T	−12	−1.02	0.14	−1.81	0.06
C7-8591-4T	0	1.53	−0.13	0.00	0.00
C7-8616-6TB	30	−1.00	0.25	1.83	0.25
C5-9261-1	55	1.30	0.06	−8.52	−0.04
C5-9229-3T	70	3.60	−0.31	−2.05	0.08
C5-9287-3T	95	−3.98	0.07	0.62	0.01
Average		0.44	0.02	−2.10	0.04

5. Conclusions

Quantitative analyses of carbides and oxides in hot-rolled coil by optical metallography and by SEM-BEI were compared. They are in reasonable agreement for maximum particle size and maximum area fraction. Both methods of analysis showed that carbide and intermetallic oxide inclusion populations in VIM-VAR hot-rolled coil varied significantly in the amount and size of inclusions with the alloy transformation temperature. Therefore, an analysis of a larger number of samples at each TTR is needed to develop statistically precise data.

All carbide inclusions were less than 12.5 μm and less than 1.0% area fraction in all samples at all TTRs. This includes samples in which there are no intermetallic oxides. The maximum size and area fraction of carbides decreases as the TTR increased.

Intermetallic oxides fractured during hot working; however, stringering was very limited. The fracturing appeared to occur in high TTR alloys, but not in low TTR alloys. This dependence on TTR suggests that the chemistry in or around the oxides affects their fracture behavior.

Chemistry and process variations within the current specifications and process definitions can have a significant effect on inclusion content. Additional limitations on manufacturing processes will be needed to make a large reduction in inclusion content with respect to current specifications.

Optical and SEM-BEI metallography can be used for quantitative evaluation of inclusions in NiTi alloys. Understanding the differences between the two methods and their respective limitations will facilitate a better use of these methods and a better understanding of the data.

References

1. ASTM F 2063-05, *Standard Specification for Wrought Nickel-Titanium Alloys for Medical Devices and Surgical Implants*, ASTM International, 2005
2. ASTM E1245-03, *Practice for Determining the Inclusion or Second Phase Constituent Content of Metals by Automatic Image Analysis*, ASTM International, 2005
3. A. Toro, F. Zhou, M.H. Wu, W. Van Geertruyden, and W.Z. Mislolek, Characterization of Non-Metallic Inclusions in Superelastic NiTi Tubes, *J. Mater. Eng. Perform.*, 2009, **18**(5–6), p 448–458
4. F. Sczerzenie et al., Comparison of Inclusions in Cold Drawn Wire and Precursor Hot Rolled Rod Coil in VIM-VAR Nickel-Titanium Alloys. SMST 2010, in Press